Properties and detection of spin nematic order in strongly correlated electron systems

Daniel Podolsky and Eugene Demler

Department of Physics, Harvard University, Cambridge, MA 02138, USA
E-mail: dpodolsky@berkeley.edu and demler@cmt.harvard.edu

Abstract. A spin nematic is a state which breaks spin SU(2) symmetry while preserving translational and time reversal symmetries. Spin nematic order can arise naturally from charge fluctuations of a spin stripe state. Focusing on the possible existence of such a state in strongly correlated electron systems, we build a nematic wave function starting from a t-J-type model. The nematic is a spin-2 operator, and therefore does not couple directly to neutrons. However, we show that neutron scattering and Knight-shift experiments can detect the spin anisotropy of electrons moving in a nematic background. We find the mean-field phase diagram for the nematic taking into account spin–orbit effects.

Contents

Institute *of* **Physics** ◑ DEUTSCHE PHYSIKALISCHE GESELLSCHAFT

1. Introduction

When ordered, classical spin systems can arrange in a number of patterns, including (anti)ferromagnetic, canted and helical structures. In addition to these, quantum mechanics allows the formation of a wealth of magnetic phases for quantum spins not available to their classical counterparts. Due to its quantum numbers, detection of such an order is often difficult: for instance, Nayak has considered a generalization of spin-density wave (SDW) order, in which spin-triplet particle–hole pairs of non-zero angular momentum condense with a modulated density [1]. These states are characterized by spin currents rather than spin densities: thus, they do not couple at linear order to probes such as photons, neutrons or nuclear spins. Only at second order do these phases couple to conventional probes, e.g. in two-magnon Raman scattering. Despite the challenges involved in their detection, subtle forms of magnetic ordering such as these may be necessary to explain phenomena such as the specific-heat anomaly in the heavy-fermion compound URu_2Si_2 [2], and the pseudogap regime in the cuprates [3].

Promising materials for the observation of exotic magnetic phases include systems with strong antiferromagnetic fluctuations such as the heavy-fermion compounds, the organic superconductors and the cuprates. For instance, the cuprates in the absence of carrier doping are antiferromagnetic Mott insulators at low temperatures. As carriers are introduced through doping, the nature of the magnetic order evolves until, for optimally doped and overdoped samples, the system becomes a metallic paramagnet. In between these two limits, the underdoped cuprates have been argued to have spin glass [4] and stripe phases [5]. The proximity between Mott insulator and superconducting phases in the cuprates makes them ideal systems to study the hierarchy by which the broken symmetry of Mott insulators is restored [6, 7].

In this paper, we will explore the possibility of detection of spin nematic order, a different quantum magnetic phase, in strongly correlated electron systems [8, 9]. Nematic order has been proposed as a state originating from charge fluctuations of stripe order [10, 11]. A spin stripe is a unidirectional collinear SDW, and it consists of antiferromagnetically ordered domains separated by anti-phase domain walls, across which the direction of the staggered magnetization flips sign. The order parameter is

$$\mathbf{S}(\mathbf{r}) = \Phi e^{i\mathbf{K}_s \cdot \mathbf{r}} + \Phi^* e^{-i\mathbf{K}_s \cdot \mathbf{r}},$$

with $\mathbf{K}_s = (\pi, \pi) + \vec{\delta}$ corresponding to antiferromagnetically ordered stripes with a period $2\pi/|\delta|$. Here, the complex vector $\Phi = e^{i\theta}\mathbf{n}$ takes its value within the manifold of ground states $S_1 \times S_2/Z_2$; the Z_2 quotient is necessary not to overcount physical configurations, as the transformation $e^{i\theta} \to -e^{i\theta}$, $\mathbf{n} \to -\mathbf{n}$ does not modify Φ. The real vector $\mathbf{n}$ gives the direction of the staggered magnetization in the middle of a domain, while the phase factor $e^{i\theta}$ specifies the location of the domain walls. A shift in θ by 2π translates the system by the periodicity of the SDW, and thus leaves the system invariant. Associated with collinear SDW order is the charge order due to modulations in the amplitude of the local spin magnetization [12], which can be described by a generalized charge density wave (CDW) order parameter

$$\delta\rho(\mathbf{r}) = \varphi e^{2i\mathbf{K}_s \cdot \mathbf{r}} + \varphi^* e^{-2i\mathbf{K}_s \cdot \mathbf{r}},$$

for some SU(2) invariant observable ρ, not necessarily the electron density. In the stripe picture, this CDW usually arises from the accumulation of holes at the domain walls.

Stripes were first observed in elastic neutron scattering experiments on the spin-1 nickelate insulator $La_{2-x}Sr_xNiO_4$, and coexistence of stripes with superconductivity was first
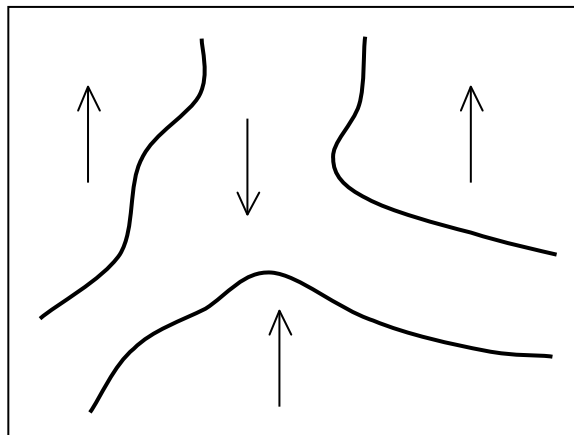
Figure 1. Charge fluctuations of a spin stripe, provided that the domain walls (curves) maintain their integrity. A spin nematic state is a linear superposition of fluctuating domain configurations such as these. Within each domain, the staggered magnetization (arrows) is well defined, and it flips sign across the anti-phase domain walls. Due to fluctuations, translational symmetry is restored to the system, and the magnetization has expectation value zero at every point. However, SU(2) symmetry is not restored, as there is a preferred axis in which spins align, modulo a sign [10, 11].

observed in underdoped $La_{1.6-x}Nd_{0.4}Sr_xCuO_4$ [13], where the unidirectional character was demonstrated by transport [14] and photoemission [15] measurements. In $YBa_2Cu_3O_{6.35}$ and $La_{1.6-x}Nd_{0.4}Sr_xCuO_4$, it is observed that SDW order is first destroyed by spin fluctuations [16]. In this case, memory of the charge modulation can remain, even after averaging over the spin direction, resulting in a spin-invariant CDW phase, whose presence may explain recent STM measurements in $Bi_2Sr_2CaCu_2O_{8+\delta}$ [17, 18].

For other materials, however, or in other regions of the phase diagram, symmetry may be restored in a different order. In particular, Zaanen and Nussinov [10, 11] proposed that many experimental features of $La_xSr_{1-x}CuO_4$ can be explained by assuming that the spin stripe order is destroyed by charge fluctuations. In this picture, dynamical oscillations in the anti-phase domain walls of a spin stripe lead to a restoration of translational symmetry and a loss of Néel order. However, although both charge and spin order seem to be destroyed in this process, $\delta\rho = 0$ and $\mathbf{S} = 0$, full spin symmetry need not be restored: so long as neither dislocations nor topological excitations of the spin proliferate, the integrity of the domain walls allows the staggered magnetization on each oscillating domain to be well defined. Thus, although the local magnetization does not have an expectation value, the magnetization modulo an overall sign does. This is nematic order, in which $\mathbf{S}$ and $-\mathbf{S}$ are identified, see figure 1. The order parameter can be chosen to be $\langle S^\alpha S^\beta - S^2\delta^{\alpha\beta}/3\rangle \propto \langle n^\alpha n^\beta - 1/3n^2\delta^{\alpha\beta}\rangle \neq 0$, which has a non-zero expectation value. Because translational invariance is restored in this process, the nematic order parameter is spatially uniform, instead of being modulated by some multiple of the SDW wave vector. In addition, we expect the nematic to be uniaxial, with a single preferred axis $\mathbf{n}$ (mod Z_2) inherited from the nearby collinear SDW.

Direct observation of spin nematic order through conventional probes is difficult. For instance, neutrons do not couple to nematic order, which is a spin-two operator. Similarly, nematic

order is translationally invariant, and does not give Bragg peaks in x-ray experiments. In principle, two-magnon Raman scattering can probe nematic order, but, in practice, it is difficult to separate the contribution due to the nematic from the creation of two magnons [10]. Hence, although spin nematic order can have important experimental consequences, e.g. for antiferromagnetic correlations in magnetic field experiments on superconducting samples [10], its direct detection remains a challenge.

The existence of other stripe liquid phases, different from the spin nematic treated in this paper, as well as proposals for their detection, are discussed in [19]. In particular, the nematic state described there originates from fluctuations of a unidirectional CDW that restore translational invariance but, by maintaining a memory of the original orientation of the CDW, break the rotational symmetry (point group) of the lattice. Hence, unlike the spin nematic, this 'charge nematic' is SU(2) spin invariant, and only breaks a discrete group.

2. Spin nematic order parameter

A spin nematic is a state that breaks spin SU(2) symmetry without breaking time reversal invariance [8, 20]. The presence of spin nematic order can be observed in the equal time spin–spin correlator

$$\langle \hat{S}^\alpha(\mathbf{r}_1)\hat{S}^\beta(\mathbf{r}_2)\rangle = C(\mathbf{r}_1, \mathbf{r}_2)\delta^{\alpha\beta} + \epsilon^{\alpha\beta\gamma}A^\gamma(\mathbf{r}_1, \mathbf{r}_2) + Q^{\alpha\beta}(\mathbf{r}_1, \mathbf{r}_2). \tag{1}$$

This expression corresponds to the SU(2) decomposition $(1) \otimes (1) \sim (0)_{\text{sym}} \oplus (1)_{\text{asym}} \oplus (2)_{\text{sym}}$. We consider the three terms appearing in equation (1) in turn. The scalar function C is explicitly spin invariant. It contains important information regarding charge order, but it does not help us in defining a nematic phase. On the other hand, the pseudovector function $\mathbf{A} = \langle \hat{\mathbf{S}}_1 \times \hat{\mathbf{S}}_2\rangle$ gives a measure of the non-collinearity of the spin vector field. However, in the case at hand, where the nematic state originates from charge fluctuations of a collinear SDW phase, we expect $\mathbf{A}$ to vanish. This is supported by the fact that, from the point of view of the Ginzburg–Landau (GL) free energy, the pseudovector $\mathbf{A}$ cannot couple linearly to any function of the SDW order parameter $\mathbf{\Phi}$. As an aside, we note that, for systems with spin-exchange anisotropy of the Dzyaloshinskii-Moriya DM form, the DM vector will couple linearly to $\mathbf{A}$, as expected from the weak non-collinearity (canting) in such systems. However, the expectation value of $\mathbf{A}$ in this case comes from explicit breaking of the spin symmetry.

Thus, all information of interest to us is contained in the symmetric spin-2 tensor $Q^{\alpha\beta}$. We define a symmetrized traceless spin correlator $\hat{Q}^{\alpha\beta}$,

$$\hat{Q}^{\alpha\beta}(\mathbf{r}_1, \mathbf{r}_2) = \tfrac{1}{2}\left(\hat{S}_1^\alpha \hat{S}_2^\beta + \hat{S}_1^\beta \hat{S}_2^\alpha\right) - \frac{\delta^{\alpha\beta}}{3}\hat{\mathbf{S}}_1 \cdot \hat{\mathbf{S}}_2 \tag{2}$$

whose expectation value yields $Q^{\alpha\beta}$ directly,

$$Q^{\alpha\beta}(\mathbf{r}_1, \mathbf{r}_2) = \langle \hat{Q}^{\alpha\beta}(\mathbf{r}_1, \mathbf{r}_2)\rangle. \tag{3}$$

Starting from an SDW state, as domain-wall fluctuations grow to destroy charge order, translational invariance is restored to the system, ensuring that $Q^{\alpha\beta}(\mathbf{r}_1, \mathbf{r}_2)$ is independent of the centre-of-mass coordinate, i.e. $Q^{\alpha\beta}(\mathbf{r}_1, \mathbf{r}_2) = Q^{\alpha\beta}(\mathbf{r}_1 + \mathbf{R}, \mathbf{r}_2 + \mathbf{R})$ for any displacement $\mathbf{R}$.

This fact alone signals the breaking of spin symmetry, since the choice of a non-trivial (i.e. not proportional to δ^{ab}) tensor $Q^{\alpha\beta}$ has been made across the system. Thus, while $Q^{\alpha\beta}(\mathbf{r}_1, \mathbf{r}_2)$ decays exponentially with distance $|\mathbf{r}_1 - \mathbf{r}_2|$ due to the absence of long-range Néel order, the onset of nematic order is reflected in the translationally invariant expectation value in the matrix-valued function (3). Since the original SDW state has a single preferred spin direction $\hat{\mathbf{n}}$, the ensuing nematic order will be uniaxial,

$$Q^{\alpha\beta}(\mathbf{r}_1, \mathbf{r}_2) = f(\mathbf{r}_1 - \mathbf{r}_2)Q_0^{\alpha\beta}, \qquad Q_0^{\alpha\beta} = (n^\alpha n^\beta - \delta^{\alpha\beta}/3)S. \qquad (4)$$

Here, we have decomposed the order parameter into three component objects: a function f describing the internal structure of the nematic, the unit vector director field $\mathbf{n}$, and the scalar magnitude S. As seen explicitly from (3), the function f is parity-symmetric, $f(\mathbf{r}) = f(-\mathbf{r})$. As will be shown below, f is dominated by the short-range antiferromagnetic correlations between spins, and therefore has a large contribution at the wave vector (π, π). By definition, we choose this contribution to be positive, $f(\pi, \pi) > 0$. With this convention, $S > 0$ corresponds to a Néel vector that is locally aligned or anti-aligned with the director field $\mathbf{n}$ (sometimes referred to as the N$^+$ phase in the literature of classical liquid crystals, see e.g. [21]), while $S < 0$ corresponds to a Néel vector that is predominantly perpendicular to $\mathbf{n}$ (the N$^-$ phase). We will show that, at low temperatures, $S > 0$ due to the local antiferromagnetic correlations, whereas, for anisotropic systems at high temperatures, a phase with $S < 0$ is possible. Finally, we note that the unidirectional SDW state (stripe phase) breaks the discrete rotational symmetry of a tetragonal lattice. This symmetry may be restored when charge fluctuations destroy the SDW state to form the nematic. In this case, $f(\mathbf{r})$ will be symmetric under rotations on the plane by $\pi/2$, $\mathbf{r} \rightarrow R_{\pi/2}\mathbf{r}$. However, if a memory of the orientation of the stripes survives the domain wall fluctuations, f will not have such symmetry, yielding a 'nematic spin-nematic', i.e. a translationally invariant system that is anisotropic in real space and in spin space.

Sections 3 and 4 will be devoted to understanding the behaviour of the three component fields of the nematic: f, $\mathbf{n}$ and S. Then, in section 5, we will explore how this detailed knowledge can be used in experimental searches for nematic order.

3. Nematic wave function

In order to explore the possible symmetry properties of the function f, we study its short-wavelength structure by explicit construction of a nematic operator on a small cluster. As is well known, it is impossible to describe nematic order in terms of a single spin-1/2 particle, as the identification of 'up' and 'down' results in a trivial Hilbert space for the spin degree of freedom. Another way to see this is that a spin-2 operator has a vanishing expectation value with respect to any spin-1/2 state, resulting in the identity $\hat{Q}_{ij}^{\alpha\beta} \equiv 0$ whenever $i = j$.

This limitation can be overcome by coarse-graining a group of spins and constructing a nematic wave function out of them. In order to preserve the underlying rotational symmetry of the system, we carry this out on square 2×2 plaquettes of spins, and use energy considerations to find the states most likely to contribute to magnetic order. We take the t-J model as a starting point, analysing the low-energy Hilbert space in a manner similar to the projected SO(5) approach of Zhang *et al* [22] or the CORE approach of Altman and Auerbach [23]. In these analyses, the lattice is first split into plaquettes. On each plaquette, the Hamiltonian is diagonalized, and the m lowest energy states $|\psi_\nu\rangle_i$ are kept, where $\nu \in \{1, \ldots, m\}$ and i labels the plaquette. For a lattice
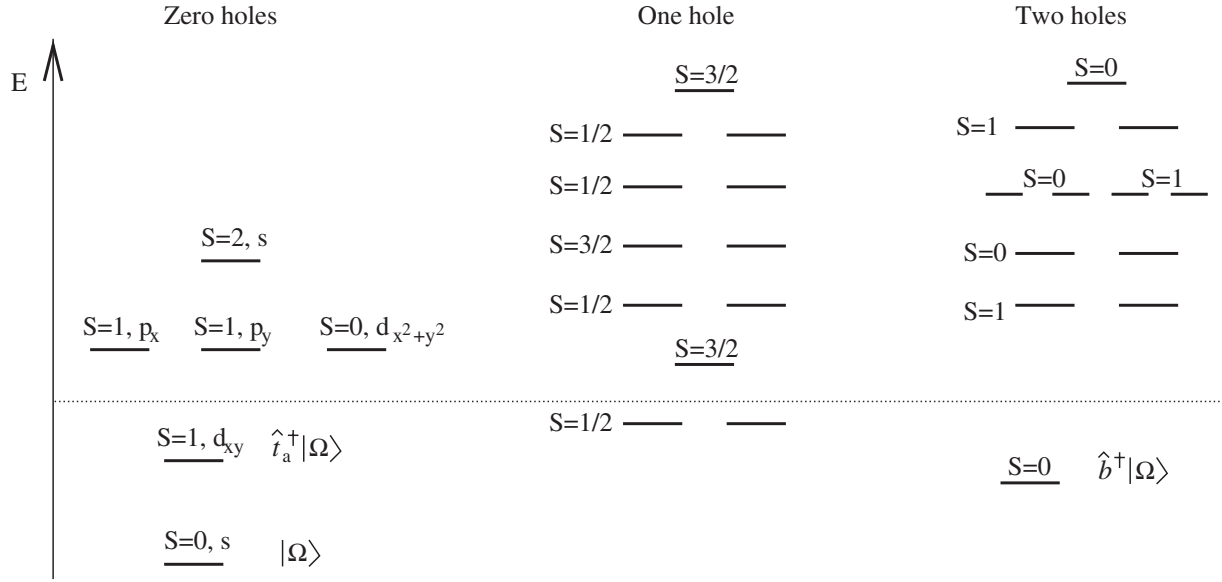
Figure 2. Spectrum of *t-J* model on a 2×2 plaquette. Adapted from [23].

composed of N plaquettes, this allows one to define a projected subspace $\mathcal{M}$ of the Hilbert space spanned by m^N factorizable states of the form $|\psi_{\nu_1}\rangle_1 \otimes |\psi_{\nu_2}\rangle_2 \cdots |\psi_{\nu_N}\rangle_N$. We assume that the ground state is well-contained in $\mathcal{M}$.

Figure 2 reproduces results in [23] for a *t-J* model on a 2×2 plaquette. The lowest energy bosonic states are, at half-filling, the $S = 0$ ground state $|\Omega\rangle$ and the $S = 1$ magnon triplet $\hat{t}_\alpha^\dagger|\Omega\rangle$ and, for a plaquette with two holes, an $S = 0$ state $\hat{b}^\dagger|\Omega\rangle$. In addition, there are two low-lying $S = 1/2$ fermion doublets with one hole; however, unbound holes are dynamically suppressed, as supported by DMRG calculations on larger lattices, and we shall exclude the one-hole sector in what follows. Then, to lowest order in the analysis, we only keep the low-lying bosonic states, in terms of which a general low-energy plaquette state can be written as

$$|\psi\rangle_i = (s + m^\alpha \hat{t}_{\alpha,i}^\dagger + c\hat{b}_i^\dagger)|\Omega\rangle_i. \tag{5}$$

It is useful to get some intuition regarding the wave functions (5). Introducing the total spin and staggered spin operators on a plaquette, $\hat{\mathbf{S}} = \hat{\mathbf{S}}_1 + \hat{\mathbf{S}}_2 + \hat{\mathbf{S}}_3 + \hat{\mathbf{S}}_4$ and $\hat{\mathbf{N}} = \hat{\mathbf{S}}_1 - \hat{\mathbf{S}}_2 + \hat{\mathbf{S}}_3 - \hat{\mathbf{S}}_4$, as well as the DM-type vector, $\hat{\mathbf{D}} = \hat{\mathbf{S}}_1 \times \hat{\mathbf{S}}_2 - \hat{\mathbf{S}}_2 \times \hat{\mathbf{S}}_3 + \hat{\mathbf{S}}_3 \times \hat{\mathbf{S}}_4 - \hat{\mathbf{S}}_4 \times \hat{\mathbf{S}}_1$, we find that

$$\hat{S}_\alpha \sim i\epsilon_{\alpha\beta\gamma}\hat{t}_\beta^\dagger\hat{t}_\gamma, \qquad \hat{N}_\alpha \sim \hat{t}_\alpha + \hat{t}_\alpha^\dagger, \qquad \hat{D}_\alpha \sim i(\hat{t}_\alpha - \hat{t}_\alpha^\dagger),$$

up to positive multiplicative factors and up to terms lying outside of the projected low-energy space. In particular, we find the expectation values on a single plaquette

$$\langle\hat{\mathbf{S}}_i\rangle \sim \mathbf{m}^* \times \mathbf{m}, \qquad \langle\hat{\mathbf{N}}_i\rangle \sim \text{Re}(s^*\mathbf{m}), \qquad \langle\hat{\mathbf{D}}_i\rangle \sim \text{Im}(s^*\mathbf{m}),$$

$$\langle\hat{b}_i\rangle \sim s^*c, \qquad \langle\hat{\mathbf{N}}_i\hat{b}_i\rangle \sim \mathbf{m}^*c. \tag{6}$$

The last two expressions describe local singlet and triplet superconductivity, respectively.

One can build a nematic on a cluster of plaquettes by choosing a factorizable state, in which $s = 0$ and **m** is a constant real vector on every plaquette,

$$|\psi_{\text{fact}}\rangle = \prod_i (m^\alpha \hat{t}_{\alpha,i}^\dagger + c\hat{b}_i^\dagger)|\Omega\rangle_i. \tag{7}$$

The constraint that **m** is real ensures that no long-range ferromagnetic or Néel orders develop, whereas nematic order does due to the SU(2)-symmetry breaking choice of the vector **m**. Note from (6) that $|\psi_{\text{fact}}\rangle$ is also a triplet superconducting state (except at half-filling, where $c = 0$). Order of this type is found, for instance, in the triplet superconducting state of quasi-one-dimensional Bechgaard salts, where the triplet superconducting order parameter is constant along the Fermi surface due to the splitting of the Fermi surface into two disjoint Fermi sheets [24].

On the other hand, in applications to materials such as the high T_c cuprates, we would like to introduce a nematic state that is a singlet superconductor, instead of triplet. For this, the use of non-factorizable states is necessary. For instance, introducing a local angle variable $\theta_i \in [0, 2\pi)$ on each plaquette, consider the state

$$|\psi_1\rangle = \int (\mathrm{d}\theta_1 \, \mathrm{d}\theta_2 \cdots) \left[\prod_i (s + m^\alpha \cos(\mathbf{Q} \cdot r_i - \theta_i)\hat{t}_{\alpha,i}^\dagger + c\hat{b}_i^\dagger)|\Omega\rangle_i \right], \tag{8}$$

where **m** is a constant real vector and **Q** is the wave vector of the underlying SDW. If the angle θ_i were held constant across the lattice, long-range SDW order would ensue. In contrast, by integrating independently over the θ_i at different sites, we introduce charge fluctuations that average out the local magnetization to zero. Hence, the state (8) has restored translational and time-reversal symmetry, with only singlet superconductivity and nematic order surviving. We note that (8) ignores correlations between spin degrees of freedom, controlled by $\hat{t}_\alpha^\dagger$, and charge degrees of freedom, controlled by $\hat{b}^\dagger$. More complex nematic wave functions that take this effect into account are given in appendix A. On the other hand, in practical calculations, one may consider a slightly simpler wave function than (8) by replacing the θ_i by local Ising variables $\sigma_i = \pm 1$ on each plaquette. This leads to the wave function

$$|\psi_2\rangle = \sum_{\{\sigma_1,\sigma_2,\ldots\}=\pm 1} \left[\prod_i (s + \sigma_i m^\alpha \hat{t}_{\alpha,i}^\dagger + c\hat{b}_i^\dagger)|\Omega\rangle_i \right]. \tag{9}$$

As before, this state has time-reversal and translational symmetries restored, with only spin nematic and superconducting orders surviving. Finally, note that in order to produce a nematic state without any type of superconductivity (singlet or triplet), it is necessary to introduce *another* fluctuating Ising variable which multiplies the term $c\hat{b}_i^\dagger$ in (9), thus randomizing the relative phase between all three components of the wave function.

Despite the fact that we have considered many different wave functions, depending on the possible coexistence of nematic order with different types of superconductivity, the analysis above allows us to make strong predictions on the dominant short-wavelength dependence of f. This is because, of all the low-energy plaquette states kept in the projected Hilbert space, only the triplet $\hat{t}_\alpha^\dagger|\Omega\rangle$ breaks SU(2) symmetry. Hence, only this state can contribute directly to the nematic order parameter. There are six different pairs $i \neq j$ of sites on a 2×2 plaquette, and the
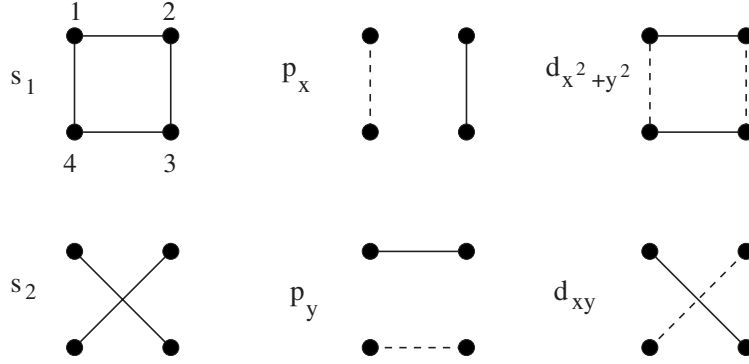
Figure 3. Basis of plaquette nematic operators with well-defined symmetry properties. The solid lines denote links with weight +1, and broken lines have weight -1. Thus, for instance, $\hat{P}_{s_1} = (\hat{Q}_{12} + \hat{Q}_{23} + \hat{Q}_{34} + \hat{Q}_{41})/2$, which in terms of the α_{ij} vectors reads $\alpha^{s_1} = (\hat{\mathbf{e}}_{12} + \hat{\mathbf{e}}_{23} + \hat{\mathbf{e}}_{34} + \hat{\mathbf{e}}_{41})/2$. The other basis vectors are $\alpha^{s_2} = (\hat{\mathbf{e}}_{13} + \hat{\mathbf{e}}_{24})/\sqrt{2}, \alpha^{p_x} = (\hat{\mathbf{e}}_{23} - \hat{\mathbf{e}}_{41})/\sqrt{2}, \alpha^{p_y} = (\hat{\mathbf{e}}_{12} - \hat{\mathbf{e}}_{34})/\sqrt{2}, \alpha^{d_{x^2+y^2}} = (\hat{\mathbf{e}}_{12} - \hat{\mathbf{e}}_{23} + \hat{\mathbf{e}}_{34} - \hat{\mathbf{e}}_{41})/2$, and $\alpha^{d_{xy}} = (\hat{\mathbf{e}}_{13} - \hat{\mathbf{e}}_{24})/\sqrt{2}$.

most general spin-2 operator $\hat{P}^{\alpha\beta}$ on a plaquette can be written as a linear combination of the six 'link' operators $\hat{Q}_{ij}$,

$$\hat{P}^{\alpha\beta} = \sum_{\{i \neq j\} \in \square} \alpha_{ij} \hat{Q}_{ij}^{\alpha\beta}. \tag{10}$$

It is useful to introduce an inner product for real functions α_{ij} on the links of a plaquette, according to $(\alpha, \beta) = \sum_{\{i \neq j\} \in \square} \alpha_{ij} \beta_{ij}$. With this, we can write a normalized basis of plaquette operators $\hat{P}_\eta$, corresponding to six linearly independent functions α_{ij}^η which satisfy $(\alpha^\eta, \alpha^\nu) = \delta^{\eta\nu}$. We choose a basis of eigenoperators of the symmetries of the plaquette, composed of operators with p_x, p_y, $d_{x^2+y^2}$ and d_{xy} symmetries, see figure 3, in addition to two operators with s-wave symmetry,

$$\hat{P}_{s_1}^{\alpha\beta} = \frac{1}{2}(\hat{Q}_{12}^{\alpha\beta} + \hat{Q}_{23}^{\alpha\beta} + \hat{Q}_{34}^{\alpha\beta} + \hat{Q}_{41}^{\alpha\beta}), \qquad \hat{P}_{s_2}^{\alpha\beta} = \frac{1}{\sqrt{2}}(\hat{Q}_{13}^{\alpha\beta} + \hat{Q}_{24}^{\alpha\beta}). \tag{11}$$

It is easy to see that among the six operators (10), only those with s-wave symmetry get a non-vanishing expectation value with respect to the state (8). What is more, the linear combination $\hat{P}_{s_F} = (\hat{P}_{s_1} + \sqrt{2}\hat{P}_{s_2})/\sqrt{3}$ has a vanishing expectation value, so that it is possible to write an orthonormal basis of operators in which only the basis operator,

$$\hat{P}_{s_A} = \frac{1}{\sqrt{3}}(-\sqrt{2}\hat{P}_{s_1} + \hat{P}_{s_2}), \tag{12}$$

has a non-zero expectation value. This can be understood as a consequence of local antiferromagnetic correlations, since $\hat{P}_{s_A}^{\alpha\beta}$ can be expressed in terms of the plaquette staggered magnetization $\mathbf{N}$ as

$$\hat{P}_{s_A}^{\alpha\beta} = \frac{1}{2\sqrt{6}}\left(N^\alpha N^\beta - \mathbf{N}^2\frac{\delta^{\alpha\beta}}{3}\right). \tag{13}$$

Using the relation

$$\hat{Q}_{ij} = \sum_{\eta} \alpha_{ij}^{\eta} \hat{P}_{\eta}, \tag{14}$$

which holds for i, j on the same plaquette, we see that the dominant short-range contribution to the nematic order parameter is

$$Q_{ij}^{\alpha\beta} = \alpha_{ij}^{s_A} \langle \hat{P}_{s_A}^{\alpha\beta} \rangle. \tag{15}$$

This is of the form (4) with

$$f(\mathbf{k}) = \alpha^{s_A}(\mathbf{k}) = \frac{4}{\sqrt{6}}(\cos k_x \cos k_y - \cos k_x - \cos k_y), \qquad Q_0^{\alpha\beta} = \langle \hat{P}_{s_A}^{\alpha\beta} \rangle. \tag{16}$$

Note that we can relate the real vector $\mathbf{m}$ in equations (8) and (9) to the director field $\mathbf{n}$ of the nematic, appearing in (4), through

$$\langle \hat{P}_{s_A}^{\alpha\beta} \rangle \propto m^{\alpha} m^{\beta} - m^2 \delta^{\alpha\beta}/3, \tag{17}$$

from which we conclude that $\mathbf{n} \propto \mathbf{m}$. This can be used to constrain the sign of S,

$$S = \tfrac{3}{2} n^{\alpha} n^{\beta} \langle \hat{P}_{s_A}^{\alpha\beta} \rangle > 0.$$

Therefore, at low temperatures, where the state of the system is dominated by the low-energy plaquette states, S is positive.

4. Mean-field analysis

We now study the finite temperature phase diagram of the spin nematic. We assume that superconductivity is either present as a background phase throughout the entire region of the phase diagram that we study or not present at all. Hence, we do not include explicitly the interaction between superconducting and nematic order parameters. As is well known (see, e.g., [25]), symmetry allows the inclusion of cubic terms into the GL free energy of a nematic order parameter. Thus, the most general GL free energy for a spin-isotropic system is, up to quartic order,

$$F_{Q,\mathrm{iso}} = \beta \mathrm{Tr} Q_0^2 - \gamma \mathrm{Tr} Q_0^3 + \delta \mathrm{Tr} Q_0^4. \tag{18}$$

By the identity $(\mathrm{Tr} Q_0^2)^2 \equiv 2\mathrm{Tr} Q_0^4$, which holds for any 3×3 traceless symmetric matrix, we do not include the term $(\mathrm{Tr} Q_0^2)^2$ in (18). The phase diagram is shown in figure 4. At high temperatures, β is large and positive, and the system is disordered, $Q_0 = 0$. On the other hand, as temperature is reduced and the value of β decreases, there is spontaneous breaking of spin SU(2) symmetry as the system undergoes a first-order transition into the nematic state. The nematic in this case is uniaxial as desired (see sections 1 and 2); in order to stabilize biaxial nematic order, terms of order Q_0^5 and Q_0^6 would have to be added to the free energy [25]. We note that, as discussed
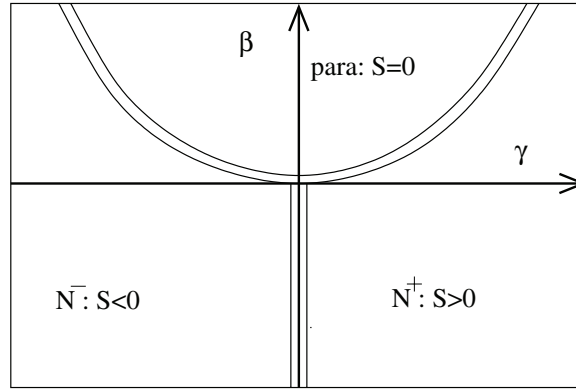
Figure 4. Mean field phase diagram for a nematic without anisotropy in the spin-exchange interaction. The ordered phases $N^{\pm}$ are uniaxial. All transitions are first order.

in sections 2 and 3, $S > 0$ in the low-temperature phase. Thus, the cubic coefficient γ must be positive.

How is the above analysis modified by the presence of spin–orbit effects? For definiteness, we concentrate on the case of the cuprate $La_xSr_{1-x}CuO_4$ in the low-temperature orthorhombic (LTO) phase. This compound displays strong evidence for fluctuating stripe order in its underdoped regime [26], and the spin-exchange constants $J^{\alpha\beta}$ are known in detail from neutron scattering experiments in undoped La_2CuO_4 [27, 28]. The analysis presented here can be easily generalized to other materials. In $La_xSr_{1-x}CuO_4$, spin–orbit effects are small: the anisotropic part of the spin-exchange interaction $J^{\alpha\beta}$ is less than 10^{-2} of the isotropic part in undoped La_2CuO_4 [27, 28]. Yet, at low temperatures, this anisotropy leads to a preferred direction for the Néel order and to weak ferromagnetism [29]. Thus, although the anisotropy is a low-energy effect, playing a weak role on the onset and magnitude of the nematic order parameter, it may ultimately fix the preferred spin orientation for the nematic. This aspect of the interplay between J and Q will be especially important when we try to separate their contributions to the anisotropy in the spin susceptibility (see equation (26) below).

The most general form of the spin-exchange interaction for spins on nearest-neighbour Cu sites is

$$
\begin{aligned}
\mathcal{H} &= \sum_{\langle ij \rangle} J_{ij}^{\alpha\beta} S_i^{\alpha} S_j^{\beta} \\
&= \sum_{\langle ij \rangle} \left(J_{0,ij} \mathbf{S}_i \cdot \mathbf{S}_j + J_{s,ij}^{\alpha\beta} S_i^{\alpha} S_j^{\beta} + \mathbf{D}_{ij} \cdot (\mathbf{S}_i \times \mathbf{S}_j) \right),
\end{aligned}
\tag{19}
$$

where $J_s^{\alpha\beta}$ is a traceless symmetric tensor and $\mathbf{D}$ is the DM vector. Neither J_0 nor J_s depend on the bond $\langle ij \rangle$. It is convenient to work with the principal axes of the system: the vectors $\mathbf{a}$ and $\mathbf{c}$ lie on the CuO_2 planes at $45°$ from nearest-neighbour Cu–Cu bonds, and the vector $\mathbf{b}$ is normal to the CuO_2 planes, see figure 5. On this basis, J_s is diagonal, $J_0 \mathbf{1} + J_s = \text{diag}(J^{aa}, J^{bb}, J^{cc})$ with $J^{bb} < J^{aa} \approx J^{cc}$ [27]. For simplicity, we take $J^{aa} = J^{cc}$ in what follows, corresponding to easy plane antiferromagnetic interactions along the $\mathbf{a}$–$\mathbf{c}$ plane. On the other hand, the DM vector $\mathbf{D}_{ij}$ points along $\pm\mathbf{a}$, with the sign on each bond $\langle ij \rangle$ given by the staggered pattern
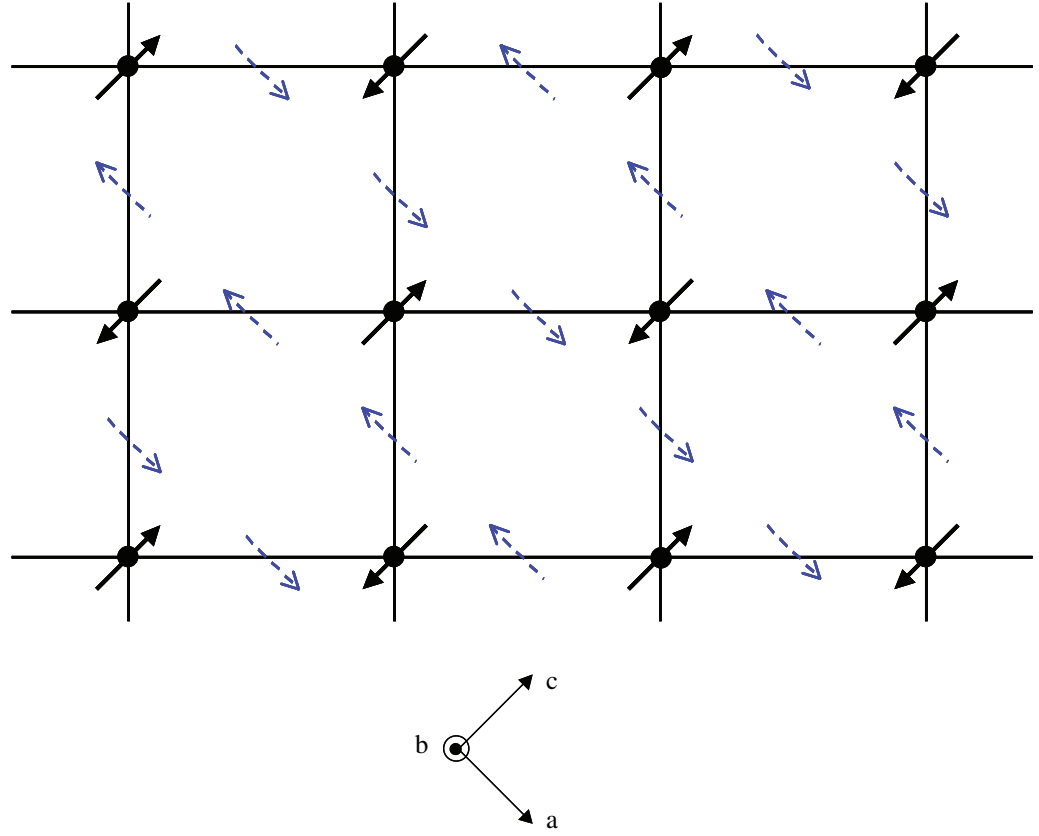
Figure 5. The DM vectors (broken arrows) and ground-state spin orientation (solid arrows) on a single CuO_2 plane in the LTO phase of La_2CuO_4. The black dots denote Cu sites. The DM vectors $\mathbf{D}_{ij}$ point along $\pm\mathbf{a}$ and are staggered between adjacent bonds. This, combined with easy plane anisotropy, yield a weakly canted AF order, where the spins on the Cu sites have a large staggered component in the $\pm\mathbf{c}$ direction, and a small uniform component out of the plane (in the $\mathbf{b}$ direction, not shown).

shown in figure 5. Thus,

$$J_{ij} = \begin{pmatrix} J_0 + \Delta & 0 & 0 \\ 0 & J_0 - 2\Delta & \pm D \\ 0 & \mp D & J_0 + \Delta \end{pmatrix},$$

where $\Delta = (J^{aa} - J^{bb})/3 > 0$. A useful measure of the relative importance of the anisotropies Δ and D is given by the ratio $x \equiv \frac{D^2}{J_0\Delta}$, which is approximately equal to 1 in the LTO phase of La_2CuO_4 [27, 28].

It is instructive to consider first the effects of spin anisotropy on an antiferromagnet. The GL free energy F_N of a Néel order parameter $\mathbf{N}$ is, to lowest order in spin–orbit coupling,

$$F_N = -\lambda\mathbf{N}^{\mathrm{T}}J_s\mathbf{N} + \frac{\lambda'}{J_0}(\mathbf{D}\cdot\mathbf{N})^2 + \mu\mathbf{N}^2 + \nu\mathbf{N}^4. \tag{20}$$

The term $\mathbf{D} \cdot \mathbf{N}$ is a pseudoscalar and is forbidden by parity and time-reversal symmetries. The first two terms include the effects of anisotropy and are both quadratic in the spin–orbit coupling. The coefficient λ is positive, as necessary to capture the tendency of spins to order along the easy plane at low temperatures. Similarly, the DM vector induces a weak canting for staggered spins that are perpendicular to it. This pushes $\mathbf{N}$ towards the plane normal to $\mathbf{D}$, which requires $\lambda' > 0$. Thus we see that J_s chooses an easy plane for the spins, and the DM vector selects a preferred direction, $\mathbf{c}$, within the easy plane [29], see figure 5. The ratio λ'/λ is unimportant in this case.

We now turn our attention to the nematic. In addition to the usual GL free energy for a nematic order parameter, equation (18), the explicit symmetry breaking due to anisotropy in the spin-exchange can be taken into account, to quadratic order in the spin–orbit interaction, by adding the terms

$$F_Q = F_{Q,\mathrm{iso}} + F_{Q,\mathrm{anis}} \qquad F_{Q,\mathrm{anis}} = -\alpha \mathrm{Tr}(J_s Q_0) + \frac{\alpha'}{J_0}\mathbf{D}^\mathrm{T} Q_0 \mathbf{D}. \qquad (21)$$

Note that, unlike the Néel case (20), the order parameter Q couples linearly to the anisotropy. Thus, the symmetry is broken explicitly and, strictly speaking, there is no disordered phase with $Q_0 = 0$. This, however, does not preclude the existence of crossovers in the order parameter, or even discontinuities at first-order transitions, as we traverse the phase diagram. For weak anisotropy, the order parameter will be extremely small at high temperatures, and very sharp crossovers will be observed. Another consequence of the linear coupling is that, unlike antiferromagnetic order which always lies on the easy plane of $J^{\alpha\beta}$, uniaxial nematic order can point either in the direction of maximal coupling of $J^{\alpha\beta}$ or in the direction of minimal coupling of $J^{\alpha\beta}$, depending on the sign of S. For the state with nematic order and $S > 0$, we expect the director field $\mathbf{n}$ to lie on the easy plane and be orthogonal to $\mathbf{D}$, i.e.be parallel to the direction that the SDW state would take in the absence of charge fluctuations. This constrains the linear coefficients appearing in (21) to be positive, $\alpha > 0$ and $\alpha' > 0$.

In order to obtain the mean field phase diagram for a spin nematic, we compare the minima of F for the director field $\mathbf{n}$ pointing along the various principal axes $\hat{\mathbf{e}}_i$. The result is shown in figure 6. The low-temperature phase N^+ is a uniaxial nematic characterized by $S > 0$ and $\mathbf{n} = \mathbf{c}$. The high-temperature phase N^- is also uniaxial, but it has $S < 0$. The director field in N^- depends on the relative strength of the two anisotropy terms, $w \equiv \alpha' x/\alpha$. This quantity is material-dependent and is unlikely to change significantly over the phase diagram (except, of course, across a structural phase transition), so that only one of the following scenarios should be observed within a given material: for $w < 1$, $\mathbf{n} = \mathbf{b}$, whereas for $w > 1$, $\mathbf{n} = \mathbf{a}$. The coefficient β increases with temperature, possibly tuning a first-order phase transition between phases N^+ and N^-, or otherwise moving the system through a sharp crossover within the N^- phase. In either case, the temperature dependence of the order parameter leads to strong experimental signatures discussed in section 5. Figure 7 shows the value of S as we move across the N^+/N^- phase transition along the broken line in figure 6.

5. Detection

In the presence of a spin nematic order parameter $Q_{ij}^{\alpha\beta} \equiv Q^{\alpha\beta}(\mathbf{r}_i, \mathbf{r}_j)$ of the form (4), symmetry allows the term

$$\mathcal{H}_{int} = -g \sum_{ij} Q_{ij}^{\alpha\beta} \hat{S}_i^\alpha \hat{S}_j^\beta \qquad (22)$$
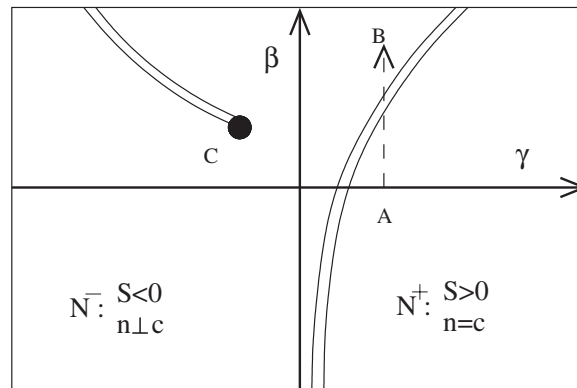
Figure 6. Mean field phase diagram including anisotropy in the spin exchange $J^{\alpha\beta}$, for the case $J^{bb} < J^{aa} = J^{cc}$, $\mathbf{D} = \pm\mathbf{a}$. All transitions are first-order. Phase N^+ is characterized by $S > 0$ and $\mathbf{n} = \mathbf{c}$, phase N^- by $S < 0$. The director $\mathbf{n}$ in phase N^- depends on the parameter $w \equiv \alpha'x/\alpha$: for $w < 1$, $\mathbf{n} = \mathbf{b}$, whereas, for $w > 1$, $\mathbf{n} = \mathbf{a}$. The parameter w is material-dependent and is unlikely to change across the phase diagram. Thus, only a single type of N^- phase is accessible within a given material. The broken arrow shows a possible trajectory where a first-order transition is crossed as temperature is increased; alternatively, for smaller values of γ, the first-order transition may be avoided and strong crossover behaviour may be observed instead.
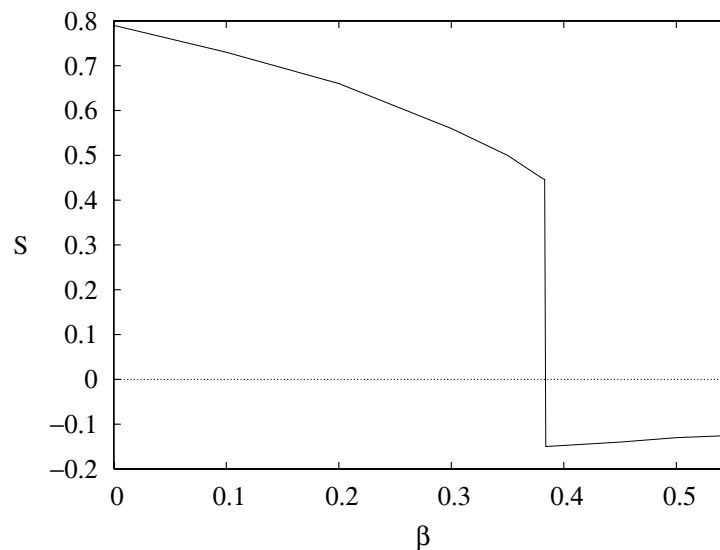

Figure 7. Value of S along the dotted trajectory in figure 6. The parameters $\alpha\Delta = 0.1$, $w < 1$ and $\gamma = \delta = 1$ are chosen for concreteness; β increases with temperature. As the anisotropy Δ is decreased, or for trajectories that start deep inside the N^+ phase due to a larger value of γ, the value of $|S|$ in the high temperature phase is reduced. Similarly, for small values of γ, the first-order transition may be avoided and instead a strong crossover within the N^- phase may be observed.

to enter the Hamiltonian, which can be thought of as a local spin–spin interaction mediated by the nematic order. The coefficient g is positive, as necessary for the stability of the nematic order. When the system develops long-range nematic order, electrons move in a nematic background which acts like an effective anisotropic spin exchange. This leads to anisotropy in the spin response function. In the random-phase approximation (RPA), when an external magnetic field **B** is applied to the system, $\mathcal{H} = \mathcal{H}_0 + \mathcal{H}_{int} - \sum_i \mathbf{B}_i \cdot \hat{\mathbf{S}}_i$, the electrons see an effective field

$$B_{\mathrm{eff}}^\alpha(\mathbf{k}) = B^\alpha(\mathbf{k}) + g Q^{\alpha\beta}(\mathbf{k})\langle \hat{S}^\beta(\mathbf{k})\rangle, \tag{23}$$

leading to the dynamic spin response

$$\chi_{\mathrm{RPA}}^{\alpha\beta}(\mathbf{k}, \omega) = \chi_0(\mathbf{k}, \omega)[(\hat{1}_{2\times 2} + g Q(\mathbf{k})\chi_0(\mathbf{k}, \omega))^{-1}]^{\alpha\beta}. \tag{24}$$

Spin nematic order thus induces anisotropy in the spin susceptibility. We introduce a tensor $\Xi^{\alpha\beta}$, defined by

$$\Xi^{\alpha\beta}(\mathbf{k}, \omega) \equiv \tfrac{1}{2}[(\chi^{-1})^{\alpha\beta} + (\chi^{-1})^{\beta\alpha}] - \frac{\delta^{\alpha\beta}}{3}\sum_c (\chi^{-1})^{cc}.$$

Experimental measurements of $\chi^{\alpha\beta}$ from polarized neutron scattering experiments (for arbitrary wave vector **k**) can be used to compute $\Xi^{\alpha\beta}$, which is the natural object to consider when studying nematic order. In the current approximation, we find

$$\Xi_{\mathrm{RPA}}^{\alpha\beta}(\mathbf{k}, \omega) = g Q^{\alpha\beta}(\mathbf{k}). \tag{25}$$

Similarly, Knight shift measurements give access to the local static spin susceptibility, i.e. the susceptibility integrated over all wave vectors **k**. To linear order in the nematic order parameter Q, the anisotropy in the Knight shift over the various principal axes α is proportional to

$$-\int \frac{\mathrm{d}^2 k}{(2\pi)^2}[\chi_0(\mathbf{k}, \omega = 0)]^2 \Xi^{\alpha\alpha}(\mathbf{k}, \omega = 0),$$

where no summation over α is implied.

Even in the absence of nematic ordering, spin–orbit coupling leads to anisotropy in the antiferromagnetic exchange $J_{ij}^{\alpha\beta}$, which enters the Hamiltonian in a term of the form (22) with $gQ \to -J$, see equation (19). The complete expression for $\Xi^{\alpha\beta}$ is therefore

$$\Xi_{\mathrm{RPA}}^{\alpha\beta}(\mathbf{k}, \omega) = g Q^{\alpha\beta}(\mathbf{k}) - J_{\mathrm{s}}^{\alpha\beta}(\mathbf{k}). \tag{26}$$

Note that only the traceless symmetric part of J_{ij} contributes to Ξ. We face the challenge of untangling the contributions to (26) due to the anisotropy in J from those coming from the presence of nematic order. For this, the analysis of section 3 is pivotal, in particular equation (16), which gives the dominant wave vector dependence of the nematic contribution to the anisotropy in the spin response function, see figure 8. This can be combined with detailed knowledge of the form of J_{s} [27, 28], $J_{\mathrm{s}}(\mathbf{k}) = \eta(\mathbf{k})\Delta \operatorname{diag}(1, 1, -2)$. As before, $\Delta = (J^{aa} - J^{bb})/3 > 0$, and we assume that anisotropy is small beyond the nearest-neighbour range to set $\eta(\mathbf{k}) = 2(\cos k_x + \cos k_y)$. Thus, the contributions due to Q and J can be distinguished by the wave vector dependence
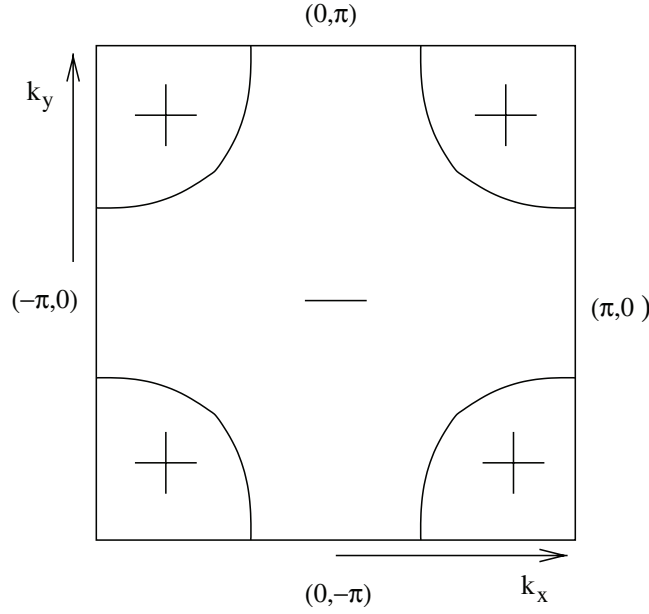
Figure 8. Wave vector dependence of $f(\mathbf{k})$ corresponding to the plaquette nematic operator $\hat{P}_{s_A}$. This is expected to be the dominant contribution to f and enters the anisotropy of the spin susceptibility through equation (26). The '+' and '−' regions show the sign of $f(\mathbf{k})$ on the Brillouin zone.

of the signal, as one is proportional to $f(\mathbf{k}) = \frac{4}{\sqrt{6}}(\cos k_x \cos k_y - \cos k_x - \cos k_y)$ and the other to $\eta(\mathbf{k}) = 2(\cos k_x + \cos k_y)$. For example, experiments measuring the susceptibility at points $\mathbf{k} = (\pi, 0)$ and $(0, \pi)$ are sensitive to Q, but not J, see figure 8.

For completeness, we evaluate the expression (26) in the various phases shown in figure 6 for underdoped La$_x$Sr$_{1-x}$CuO$_4$. In the low-temperature phase N$^+$, we expect that

$$\Xi^{aa} = -g|S|f(\mathbf{k})/3 - \Delta\eta(\mathbf{k}),$$

$$\Xi^{bb} = -g|S|f(\mathbf{k})/3 + 2\Delta\eta(\mathbf{k}),$$

$$\Xi^{cc} = 2g|S|f(\mathbf{k})/3 - \Delta\eta(\mathbf{k}).$$

In the high-temperature phase N$^-$, we must consider two separate scenarios. If $w > 1$, then $\mathbf{n} = \mathbf{a}$, and

$$\Xi^{aa} = -2g|S|f(\mathbf{k})/3 - \Delta\eta(\mathbf{k}),$$

$$\Xi^{bb} = g|S|f(\mathbf{k})/3 + 2\Delta\eta(\mathbf{k}),$$

$$\Xi^{cc} = g|S|f(\mathbf{k})/3 - \Delta\eta(\mathbf{k}),$$

whereas, if $w < 1$, then $\mathbf{n} = \mathbf{b}$, and

$$\Xi^{aa} = -\Xi^{bb}/2 = \Xi^{cc}, \qquad \Xi^{cc} = g|S|f(\mathbf{k})/3 - \Delta\eta(\mathbf{k}).$$

Thus, if the system goes through a phase transition between phases N$^+$ and N$^-$, the discontinuity in S, shown in figure 7, together with the change in the director field $\mathbf{n}$, would give a very clear experimental signature of nematic order in Knight shift and polarized neutron scattering experiments.

Finally, we consider the prospect of observing director density waves (DDW), the Goldstone modes corresponding to the nematic state, in neutron scattering experiments. To do this, we study the pole structure of the RPA result (24). Expanding (24) about $\mathbf{k} = 0$ and $\omega = 0$, we find two degenerate DDW modes, with speed $v_{\text{DDW}} \propto \sqrt{g|S|}$,

$$\chi^{\perp\perp}(\mathbf{k}, \omega) \propto \frac{\mathbf{k}^2}{\omega^2 - v_{\text{DDW}}^2 \mathbf{k}^2}, \tag{27}$$

with $\perp$ labelling either of the directions perpendicular to the director of the nematic. Equation (27) is consistent with an independent calculation of the DDW modes starting from an effective low-energy quantum rotor model, see section 6. We note that the DDW modes found here may be overdamped, depending on the details of the system. This would be the case, for instance, if v_{DDW} were smaller than the Fermi velocity. However, provided that the modes are underdamped, they can be detected in neutron scattering experiments. This is surprising at first, as local Z_2 invariance implies that equal-time correlators of the from $\langle S_i^\alpha S_j^\beta \rangle$ must decay exponentially at large distances $|\mathbf{x}_i - \mathbf{x}_j|$. However, as (27) indicates, the correlator at different times need not decay exponentially. Also note that the inelastic scattering peak (27) has vanishing weight as $\mathbf{k} \to 0$, consistent with the absence of an elastic Bragg peak. Unfortunately, this feature makes DDW modes difficult to distinguish from the low-energy collective modes of a quantum paramagnet, computed in appendix B.

6. Quantum rotor model

Another approach to study Goldstone modes is to introduce a quantum rotor model which captures the low-energy properties of the system. This can be done by coarse-graining spins in plaquettes, as carried out in section 3. There we found that the low-energy plaquette states at half-filling contain one singlet ground state, and one triplet state obtained by acting on the ground state by the staggered magnetization operator. This matches the low-energy spectrum of a quantum rotor $\hat{\mathbf{n}}_i$ on the plaquette i, which can be written in terms of the component spins of the plaquette as

$$\hat{\mathbf{L}}_i = \hat{\mathbf{S}}_{i1} + \hat{\mathbf{S}}_{i2} + \hat{\mathbf{S}}_{i3} + \hat{\mathbf{S}}_{i4}, \qquad \hat{\mathbf{n}}_i \sim \hat{\mathbf{S}}_{i1} - \hat{\mathbf{S}}_{i2} + \hat{\mathbf{S}}_{i3} - \hat{\mathbf{S}}_{i4}.$$

Here, the total spin $\hat{\mathbf{L}}$ acts as the canonical conjugate of $\hat{\mathbf{n}}$, satisfying the commutation relations

$$\left[L_i^\alpha, L_j^\beta \right] = \mathrm{i}\delta_{ij}\epsilon^{\alpha\beta\gamma} L_i^\gamma, \qquad \left[L_i^\alpha, n_j^\beta \right] = \mathrm{i}\delta_{ij}\epsilon^{\alpha\beta\gamma} n_i^\gamma, \qquad \left[n_i^\alpha, n_j^\beta \right] = 0. \tag{28}$$

We introduce an effective Hamiltonian for these rotors, consistent with local Z_2 symmetry,

$$H_{\text{rotor}} = \frac{\nu}{2} \sum_i \hat{\mathbf{L}}_i^2 - \tilde{g} \sum_{\langle ij \rangle} (\hat{\mathbf{n}}_i \cdot \hat{\mathbf{n}}_j)^2. \tag{29}$$

The dynamic spin susceptibility can be obtained, in the long-wavelength limit $\mathbf{k} \to 0$, by the linear response of $\mathbf{L}$ to an external field $\mathbf{B}_i = \mathbf{B}e^{-\mathrm{i}(\omega t - \mathbf{k} \cdot \mathbf{r}_i)}$,

$$H_{\mathbf{B}}^0 = -\sum_i \mathbf{B}_i \cdot \hat{\mathbf{L}}_i. \tag{30}$$

Institute *of* **Physics** Φ DEUTSCHE PHYSIKALISCHE GESELLSCHAFT

The Heisenberg equations of motion for the rotors become

$$\frac{d\hat{\mathbf{L}}_i}{dt} = \tilde{g} \sum_{j \in NN(i)} (\hat{\mathbf{n}}_i \cdot \hat{\mathbf{n}}_j)(\hat{\mathbf{n}}_i \times \hat{\mathbf{n}}_j) + \mathbf{B}_i \times \hat{\mathbf{L}}_i, \qquad \frac{d\hat{\mathbf{n}}_i}{dt} = \frac{v}{2}(\hat{\mathbf{L}}_i \times \hat{\mathbf{n}}_i - \hat{\mathbf{n}}_i \times \hat{\mathbf{L}}_i) - \mathbf{B}_i \times \hat{\mathbf{n}}_i. \quad (31)$$

In the absence of an external field **B**, the rotor correlator is assumed to be highly local,

$$\langle \hat{n}_i^\alpha \hat{n}_j^\beta \rangle_0 = \delta_{ij}(\delta^{\alpha\beta} n^2/3 + Q^{\alpha\beta}) \equiv \delta_{ij} G^{\alpha\beta}.$$

The product of $\hat{n}$ operators then differs from the mean field result by a correction,

$$\hat{n}_i^\alpha \hat{n}_j^\beta - \delta_{ij} G^{\alpha\beta} = \delta_{ij} \rho^{\alpha\beta} + \lambda_{ij}^{\alpha\beta},$$

which has been split into a local term $\rho^{\alpha\beta}$ and a non-local term $\lambda_{ij}^{\alpha\beta} = 0$ for $i = j$. Linearizing the equations of motion (31) with respect to these corrections, we obtain

$$-i\omega L^\alpha = F(\mathbf{k})\epsilon^{\alpha\beta\gamma} G^{\beta\delta} \rho^{\gamma\delta}, \qquad -i\omega \rho^{\alpha\beta} = (\epsilon^{\beta\gamma\delta} G^{\alpha\delta} + \epsilon^{\alpha\gamma\delta} G^{bd})(vL^\gamma - B^\gamma), \quad (32)$$

where

$$F(\mathbf{k}) = 2\tilde{g} \sum_{i=1}^{d}(1 - \cos q_i). \quad (33)$$

Since we are interested in the linear response, we have excluded from equation (32) terms quadratic in **B**. Note that, to this order in **B**, the non-local term λ_{ij} drops out of the equations of motion.

For the current case of interest, a uniaxial nematic $G^{\alpha\beta}$ is of the form

$$G = \frac{1}{3}\begin{pmatrix} n^2 - S & 0 & 0 \\ 0 & n^2 - S & 0 \\ 0 & 0 & n^2 + 2S \end{pmatrix}.$$

Solving (32) for **L** yields

$$L^\perp = -\frac{SF(\mathbf{k}^2)}{\omega^2 - vS^2 F(\mathbf{k})} B^\perp, \qquad L^{\hat{n}} = 0, \quad (34)$$

where $\perp$ is either of the directions perpendicular to $\hat{\mathbf{n}}$. Note that, unlike the case of antiferromagnetic order, $\chi^{\alpha\beta}$ has no off-diagonal contributions. This is attributed to time reversal invariance. For long wavelengths $\mathbf{k} \to 0$, $F(\mathbf{k}) \to \tilde{g}\mathbf{k}^2$, and poles in the susceptibility indicate the presence of two degenerate DDW modes, with velocity $v_{\text{DDW}} = \sqrt{vS^2\tilde{g}}$. This is consistent with the RPA result found above, see equation (27).

Finally, we compute the dynamic spin susceptibility near $k = (\pi, \pi)$ by replacing the term $H_{\mathbf{B}}^0$ by a source that couples directly to the staggered magnetization,

$$H_{\mathbf{B}}^\pi = -\sum_i \mathbf{B}_i \cdot \hat{\mathbf{n}}_i. \quad (35)$$
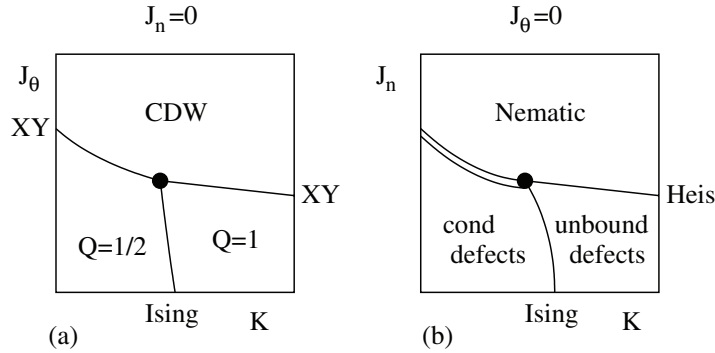
Figure 9. (a) Phase diagram for equation (37) for the case $J_n = 0$, corresponding to a Z_2 lattice gauge theory with a U(1) field. The Ising transition as K is increased corresponds to a binding of $Q = 1/2$ topological excitations into $Q = 1$ excitations. (b) Case $J_\theta = 0$, corresponding to a Z_2 lattice gauge theory with an $SO(3)$ field. The first-order nematic to paramagnetic transition can be split into two second-order transitions, passing through a topologically ordered phase.

Proceeding as above, we find the linear response

$$n_i = \frac{-vG^{\alpha\beta}}{\omega^2 - z\tilde{g}n^2}B_i^{\beta}, \tag{36}$$

where $z = 4$ is the coordination number of the lattice. Note that, in the current approximation, the collective modes near (π, π) are non-dispersing and gapped. The spin gap $\omega = \sqrt{z\tilde{g}n^2}$ indicates that there is no long-range Néel order in the system.

7. Lattice gauge theory

Up to now, we have ignored the possibility of fractionalization and the richer phase structure that it allows. As an example, by introducing a disclination core energy, it is possible to split the phase transition for the onset of nematic order, which is strongly first order in Landau theory, into two second-order transitions [30]. For a theory with local Z_2 gauge redundancy, it is useful to discretize the magnetic degrees of freedom on a lattice and to introduce an auxiliary gauge field $\sigma_{ij} = \pm 1$ living on the bonds of the lattice. Under a gauge transformation at site i, the site variables pick up a minus sign, $\mathbf{n}_i \to -\mathbf{n}_i$ and $e^{i\theta_i} \to -e^{i\theta_i}$, while simultaneously the bond variables surrounding i change sign, $\sigma_{ij} \to -\sigma_{ij}$. The simplest gauge invariant action that can be written under these conditions is

$$S = -J_n \sum_{\langle ij \rangle} \mathbf{n}_i \sigma_{ij} \mathbf{n}_j - J_\theta \sum_{\langle ij \rangle} \sigma_{ij} \cos(\theta_i - \theta_j) - K \sum_{\square} \prod_{\square} \sigma_{ij}. \tag{37}$$

Unlike section 4, here we ignore the anisotropy in the tensor $J^{\alpha\beta}$, which is weak and only affects the very-low-energy physics. Figures 9 and 10 present the phase diagrams for extreme values of the couplings J_n, J_θ and K. Figure 9 shows the phase diagrams for the cases $J_n = 0$ and $J_\theta = 0$.

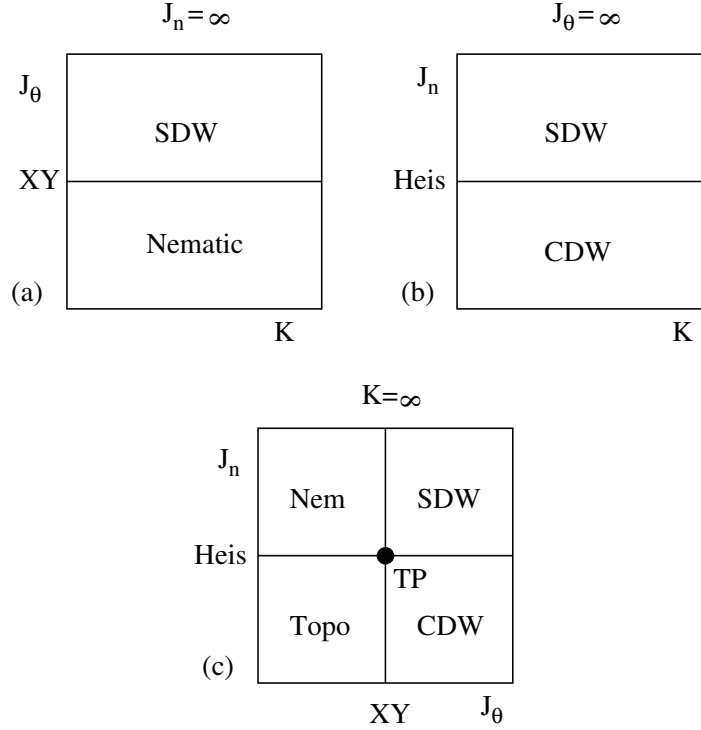Institute *of* **Physics** ✆DEUTSCHE PHYSIKALISCHE GESELLSCHAFT

Figure 10. Phase diagrams when any of the couplings in equation (37) is infinite. In all these cases, topological defects in the gauge field are energetically forbidden, and we can work in minimal gauge $\sigma_{ij} = 1$. (a) Case $J_n = \infty$, ensures that at least nematic order is present. K is irrelevant in this situation, as the field σ_{ij} is frozen. As J_θ is increased, the system undergoes an XY transition from nematic to SDW order. The situation is similar to the case $J_\theta = \infty$, shown in (b), but now a Heisenberg transition is seen from CDW to SDW order. In (c), $K = \infty$, leading to a dynamical decoupling of the θ and $\mathbf{n}$ terms in the action (37). For small J_θ and $J_\mathbf{n}$ values, a paramagnet with only topological order survives.

These correspond to Z_2 lattice gauge theories with U(1) and SO(3) Higgs fields, respectively, which have been studied extensively in the literature [30]–[33].

Figure 10 shows the situation when any of the couplings in (37) is infinite. In all these cases, the auxiliary field σ_{ij} is completely ordered, and we can work in 'minimal gauge', where $\sigma_{ij} = 1$ for all bonds. This corresponds to a lack of topological defects, which are energetically forbidden. Once a value of $\mathbf{n}$ (or θ) is chosen at a given lattice point, smoothness of the fields ensures that the Z_2 redundancy in $\mathbf{n}$ (θ) is removed everywhere. Thus, the universality class of these transitions is the same as that of the corresponding ungauged theories. For instance, in figure 10(c), starting with the topologically ordered paramagnet at small J_n and J_θ, we can increase J_θ until the onset of CDW order through an XY phase transition. Similarly, by increasing J_n, we get the onset of nematic order through a Heisenberg transition. In these regions of phase space, the simultaneous presence of both CDW and nematic orders imply SDW order. To see this, suppose that $\langle \mathbf{n} \rangle_m$ and $\langle e^{i\theta} \rangle_m$ are simultaneously non-zero, where the subscript m indicates that we are working in minimal gauge. Then, $\langle e^{i\theta} \mathbf{n} \rangle_m$ is non-zero, but this quantity is in fact independent of the gauge used. The results of figures 9 and 10 are combined in figure 11.
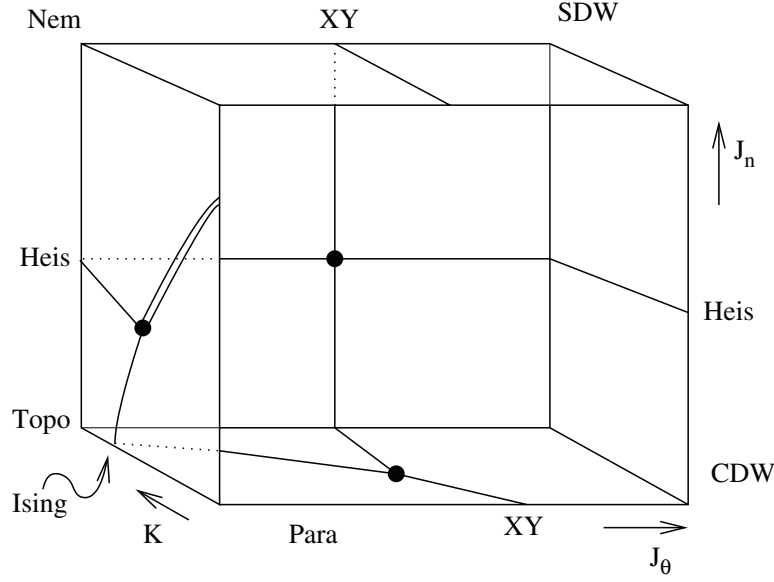
Figure 11. Five faces of the phase diagram of the action (37): $J_\theta = 0$, $J_\theta = \infty$, $J_n = 0$, $J_n = \infty$ and $K = \infty$. We do not compute the phase diagram along the sixth face, $K = 0$, explicitly. However, there are indications from *XY* spins in 2D that the only phases present there are paramagnetic, CDW, SDW and nematic [34]. However, introduction of a new term (39) can spit the SDW into a CDW+nematic phase. Note that, for large values of K, a topologically ordered phase becomes available.

Let us now consider the phase diagram when $K = 0$. In this case, the auxiliary gauge field fluctuates strongly, and it is useful to sum (37) over σ_{ij} configurations to get

$$S_{\text{eff}} = -\frac{J_n^2}{2} \sum_{\langle ij \rangle} (\mathbf{n}_i - \mathbf{n}_j)^2 - \frac{J_\theta^2}{2} \sum_{\langle ij \rangle} \cos^2(\theta_i - \theta_j)$$
$$- J' \sum_{\langle ij \rangle} \mathbf{n}_i \cdot \mathbf{n}_j \cos(\theta_i - \theta_j) + \cdots. \tag{38}$$

In this particular model, $J' = J_n J_\theta$. An analysis of two-dimensional algebraic order in a model of this sort (with *XY* spins) has been carried out in [34]. There, the only phases present are paramagnet, CDW, nematic and SDW, and there is a direct transition between paramagnetic and SDW phases. Thus, for the action (37), although we only look at the boundary of the phase diagram , in all the limits considered, the simultaneous appearance of nematic and CDW order implies SDW order.

However, it is possible to have a state with nematic and CDW orders without simultaneously stabilizing SDW order. To see this, notice that J' in (38) can be tuned by adding an extra gauge invariant term to the original action (37)

$$\Delta S = -J_e \sum_{\langle ij \rangle} \mathbf{n}_i \cdot \mathbf{n}_j \cos(\theta_i - \theta_j). \tag{39}$$

In particular, when $J' = 0$, equation (38) leads to two independent transitions for $\mathbf{n}$ and θ, yielding paramagnetic, CDW, nematic and nematic + CDW phases. The latter phase breaks SU(2) spin symmetry and translational symmetry, but leaves time reversal invariant. How can such a state arise from fluctuations of a spin stripe? In the stripe picture, an anti-phase domain wall serves a dual role, both as a region where charge accumulates and as a boundary between domains of opposite staggered magnetization. The effect of (39) is to disentangle these two roles to obtain two separate objects, a charge line component and a magnetic anti-phase line component. Then, fluctuations of the anti-phase line component can restore time reversal symmetry without restoring translational invariance. Note that, as the extra coupling J_e is decreased, an Ising phase transition between nematic+CDW and SDW phases begins to occur in the corner of the phase diagram $J_\theta, J_n \to \infty$ until, for small enough J_e, the nematic+CDW phase disappears entirely in favour of the SDW phase.

8. Summary

In this paper, we have considered the prospect of direct detection of a quantum spin nematic in strongly correlated electron systems, such as heavy-fermion compounds, the cuprates and the organic superconductors. The spin nematic order parameter is a spin-2 operator, and it does not couple, to linear order, to many of the conventional probes such as neutrons, photons or nuclear spins. However, we show that electrons moving in a nematic background have an anisotropic spin susceptibility, which can be detected in polarized neutron scattering and Knight shift experiments. In addition, we discuss the possibility of observing the Goldstone modes associated with nematic ordering in inelastic neutron scattering experiments.

In section 2, we defined the nematic order parameter in terms of the equal-time spin-correlation function, and argued for uniaxial nematic order in systems with collinear spin correlations. In section 3, we introduced wave functions to describe nematic order in a number of situations, including a stand-alone nematic, and nematic order coexisting either with spin-singlet or spin-triplet superconductivity. In order to do this, we followed a coarse-graining and low-energy projection procedure, as was done in [22, 23]. We used these wavefunctions to constrain the short-distance and low-energy structure of the nematic order parameter. In section 4, we considered the finite temperature phase diagram of the nematic through a mean-field analysis of the GL free energy. Here, we included the effects of the spin–orbit interaction which, even when weak, ultimately fix the director of the nematic. We illustrated this principle using spin-exchange constants measured in undoped La_2CuO_4. In section 5, we computed the anisotropic spin response of electrons in the nematic phase, and discussed prospects for its observation. There, we also computed the spectrum of Goldstone modes of a quantum spin nematic. In section 6, these results were supported by the analysis of an effective quantum rotor model. Finally, in section 7, we considered the possible presence of topologically ordered phases, as well as an exotic CDW+nematic phase, in a system of fractionalized electrons.

Before concluding, we would like to mention a few experimental systems where nematic order may be found (in addition to $La_xSr_{1-x}CuO_4$, which is discussed in the introduction [10, 11]). In particular, heat capacity measurements in two-dimensional solid ^3He support the presence of large many-spin interactions [35]. On the other hand, numerical simulations of spins on a square lattice with ring exchange indicate a stable 'p-nematic' phase [36]. In this case, frustration due to the ring exchange can destroy antiferromagnetic order in favour of a nematic phase. Another experimental system of interest is V_2O_3, which, as temperature and pressure are varied, displays

Institute *of* **Physics** Φ DEUTSCHE PHYSIKALISCHE GESELLSCHAFT

a Mott transition along a first-order line ending in a second-order critical point [37]. The lattice constants change discontinuously across the first-order line, leading to a change in the ratio of potential to kinetic energies, and thus to a metal-insulator transition. The topology of the phase diagram is the same as that shown in the N^- phase surrounding point C in figure 6. In fact, as discussed in section 4, spin nematic ordering couples linearly to the anisotropy in the spin exchange. Thus, discontinuity in the spin nematic order parameter leads to a discontinuous deformation of the lattice, which could explain the phase diagram of V_2O_3.

Acknowledgments

Appendix A. Correlations of spin and charge

While equation (8) gives the simplest wave function that describes a state with both superconducting and nematic orders, it does not incorporate correlations between charge and spin degrees of freedom. In the stripe picture, domain walls are not only regions where holes accumulate, they are also regions across which the staggered magnetization changes sign. One can modify (8) to include this effect, by relating σ_i to the number of domain walls crossed:

$$|\psi_3\rangle = \sum_{\{\sigma_1,\sigma_2,\ldots\}=\pm1} \prod_k \delta\left(\sigma_k - \sigma_1(-1)^{\sum_{j=1}^k \hat{b}_j^\dagger \hat{b}_j}\right) g[\hat{b}_j^\dagger \hat{b}_j]\left[\prod_i (s + \sigma_i m^\alpha \hat{t}_{\alpha,i}^\dagger + c\hat{b}_i^\dagger)|\Omega\rangle_i\right]. \quad \text{(A.1)}$$

In this case, the sum over sites inside the delta function runs over a path on the plane joining site 1 to site k. This forces a change of sign in σ_k every time a new domain wall intervenes between those two sites. The path sum is only independent of path whenever the domain walls run continuously through the sample instead of ending up abruptly, and when an odd number of them do not intersect, as would happen, for instance, in a 'T-junction'. The functional g is chosen to destroy all configurations that violate these constraints, thus enforcing the integrity of the fluctuating domain walls. The simplest choice for g is a projection operator that gives equal weight to all the allowed configurations. In this case, the wave function (A.1) can be rewritten as

$$|\psi_4\rangle = \sum_{\mathcal{D}} \prod_{i\notin\mathcal{D}} (s + \sigma_{\mathcal{D},i} m^\alpha \hat{t}_{\alpha,i}^\dagger)|\Omega\rangle_i \prod_{j\in\mathcal{D}} c\hat{b}_j^\dagger|\Omega\rangle_j, \quad \text{(A.2)}$$

where $\mathcal{D}$ denotes an allowed domain-wall configuration and $\sigma_{\mathcal{D},i}$ is the sign of the staggered magnetization on site i in configuration $\mathcal{D}$. Equations (A.1) and (A.2) are alternative descriptions of the nematic state of Zaanen and Nussinov [10, 11].

Appendix B. Collective modes of a quantum paramagnet

We would like to see if the DDW of a nematic state can be easily distinguished from the collective modes of a quantum paramagnet. These latter modes can be derived, in the RPA approximation,

by substituting $-gQ_{ij}^{\alpha\beta} \rightarrow J_0\delta^{\alpha\beta}\eta_{ij}$ in equations (22) and (24). Here, η_{ij} is equal to 1 if i and j are nearest neighbours, and zero otherwise; and $J_0 > 0$ is the antiferromagnetic spin exchange. We find an isotropic spin response

$$\chi_{\mathrm{RPA}}^{\alpha\beta}(\mathbf{k}, \omega) = \frac{\chi_0(\mathbf{k}, \omega)}{1 - J_0\eta(\mathbf{k})\chi_0(\mathbf{k}, \omega)}\delta^{\alpha\beta}, \tag{B.1}$$

where $\eta(\mathbf{k}) = 2(\cos k_x + \cos k_y)$. In the limit $\mathbf{k} \rightarrow 0$, $\omega \rightarrow 0$, the free spin susceptibility tends to $\chi_0 \rightarrow k^2/\omega^2$, leading to the long wavelength result

$$\chi_{\mathrm{RPA}}^{\alpha\beta} \sim \frac{k^2}{\omega^2 - 4J_0k^2}\delta^{\alpha\beta}.$$

Thus, there are three degenerate gapless paramagnon poles (with vanishing weight at $\mathbf{k} = 0$). On the other hand, the poles of equation (B.1) near $\mathbf{k} = (\pi, \pi)$ have a spin gap Δ due to the lack of long-range Néel order,

$$\omega_{\mathbf{k}\sim(\pi,\pi)} = \sqrt{4J_0^2(\mathbf{k} - (\pi, \pi))^2 + \Delta^2}. \tag{B.2}$$

References

[1] Nayak C 2000 *Phys. Rev.* B **62** 4880
[2] Chandra P, Coleman P, Mydosh J A and Tripathi V 2002 *Nature* **417** 831
[3] Chakravarty S, Laughlin R B, Morr D K and Nayak C 2001 *Phys. Rev.* B **63** 094503
[4] Keimer B, Birgeneau R J, Cassanho A, Endoh Y, Erwin R W, Kastner M A and Shirane G 1991 *Phys. Rev. Lett.* **67** 1930
[5] Emery V J, Kivelson S A and Tranquada J M 1999 *Proc. Natl Acad. Sci. USA* **96** 8814
[6] Sachdev S 2003 *Rev. Mod. Phys.* **75** 913
[7] Sachdev S 2003 *Ann. Phys.* (NY) **303** 226
[8] Andreev A F and Grishchuk I A 1984 *Sov. Phys.—JETP* **60** 267
[9] Gorkov L P and Sokol A V 1990 *JETP Lett.* **52** 504
[10] Zaanen J and Nussinov Z 2003 *Phys. Status Solidi* b **236** 332
[11] Nussinov Z and Zaanen J 2002 *J. Phys. (Paris) IV* **12** Pr9 245
[12] Zachar O, Kivelson S A and Emery V J 1998 *Phys. Rev.* B **57** 1422
[13] Tranquada J M, Sternlieb B J, Axe J D, Nakamura Y and Uchida S 1995 *Nature* **375** 561
[14] Noda T, Eisaki H and Uchida S 1999 *Science* **286** 265
[15] Zhou X J, Bogdanov P, Kellar S A, Noda T, Eisaki H, Uchida S, Hussain Z and Shen Z-X 1999 *Science* **286** 268
[16] Mook H, Dai P and Dogan F 2002 *Phys. Rev. Lett.* **88** 97004
[17] Hoffman J, Hudson E W, Lang K M, Madhavan V, Eisaki H, Uchida S and Davis J 2002 *Science* **295** 446
[18] Howald C, Eisaki H, Kaneko N and Kapitulnik A 2003 *Phys. Rev.* B **67** 014533
[19] Kivelson S, Blindloss I, Fradkin E, Oganesyan V, Tranquada J, Kapitulnik A and Howald C 2003 *Rev. Mod. Phys.* **75** 1201
[20] Barzykin V, Gor'kov L and Sokol A 1991 *Europhys. Lett.* **15** 869
[21] de Gennes P and Prost J 1993 *The Physics of Liquid Crystals* (Oxford: Oxford University Press)
[22] Zhang S, Hu J, Arrigoni E, Hanke W and Auerbach A 1999 *Phys. Rev.* B **60** 13070
[23] Altman E and Auerbach A 2002 *Phys. Rev.* B **65** 104508

Institute *of* **Physics** Φ DEUTSCHE PHYSIKALISCHE GESELLSCHAFT

[24] Podolsky D, Altman E, Rostunov T and Demler E 2004 *Phys. Rev. Lett.* **93** 246402
[25] Chaikin P and Lubensky T C 2000 *Principles of Condensed Matter Physics* (Cambridge: Cambridge University Press)
[26] Fujita M, Yamada K, Hiraka H, Gehring P M, Lee S H, Wakimoto S and Shirane G 2002 *Phys. Rev. B* **65** 064505
[27] Peters C J *et al* 1988 *Phys. Rev. B* **37** 9761
[28] Thio T, Thurston T R, Preyer N, Picone P, Kastner M A, Jenssen H P, Gabbe D, Chen C, Birgeneau R and Aharony A 1988 *Phys. Rev. B* **38** 905
[29] Coffey D, Bedell K and Trugman S 1990 *Phys. Rev. B* **42** 6509
[30] Lammert P, Rokhsar D and Toner J 1993 *Phys. Rev. Lett.* **70** 1650
[31] Sedgewick R D, Scalapino D J and Sugar R L 2002 *Phys. Rev. B* **65** 54508
[32] Senthil T and Fisher M P A 2000 *Phys. Rev. B* **62** 7850
[33] Demler E, Nayak C, Kee H-Y, Kim Y B and Senthil T 2002 *Phys. Rev. B* **65** 155103
[34] Krüger F and Scheidl S 2002 *Phys. Rev. B* **89** 095701
[35] Ishida K, Morishita M, Yawata K and Fukuyama H 1997 *Phys. Rev. Lett.* **79** 3451
[36] Läuchli A, Domenge J C, Lhuillier C, Sindzingre P and Troyer M 2004 *Preprint* cond-mat/0412035
[37] Limelette P, Georges A, Jérome D, Wzietek P, Metcalf P and Honing J M 2003 *Science* **302** 89